Laser and Particle Beams (2016), *34*, 193–201.

doi:10.1017/S026303461600001X

Bubble structure in laser wake-field acceleration

ERSHAD SADEGHI TOOSI,[1] SAEED MIRZANEJHAD,[2] AND DAVOUD DORRANIAN[1]

[1]Plasma Physics Research Center, Science and Research Branch, Islamic Azad University, Tehran, Iran
[2]Department of Atomic and Molecular Physics, Faculty of Basic Science, University of Mazandaran, Babolsar, Iran

(Received 23 August 2015; Accepted 23 December 2015)

Abstract

Highly nonlinear ellipsoid bubble regime of the laser wake-field acceleration with high-intensity laser pulse is considered with analytical and numerical calculations. The important property of this regime is the production of the mono-energetic high-quality electron beam. We introduce a new twofold ellipsoid structure of the bubble (egg shape) by referring to some published two-dimensional (2D) and 3D simulations. In this paper, a new analytical formalism is introduced, in which dimensions of the front part of the ellipsoid bubble are related to the laser pulse and plasma parameters. These relationships are in agreement with 2D particle-in-cell code results in recent work (Benedetti *et al.*, 2013).

Keywords: Ellipsoid bubble regime; Laser wake-field acceleration

1. INTRODUCTION

The three-dimensional (3D) highly nonlinear regime of laser wake-field acceleration (LWFA) in ultra-high laser pulse intensities is called the bubble regime (Pukhov & Meyer-Ter-vehn, 2002; Kostyukova *et al.*, 2004). In this regime, the plasma electrons are expelled by the pondermotive force of the laser pulse, and the electron-free region (bubble) is created behind the laser pulse. This regime is reached when the waist w_0 of the focused laser pulse becomes matched to the plasma parameter ($k_p w_0 \approx \sqrt{a_0}$; with $k_p = 2\pi/\lambda_p \approx \omega_p/c$, where ω_p is the plasma frequency) and when the pulse length is of the order of half-plasma wavelength ($l_p = c\tau \approx \lambda_p/2$). In addition, the laser intensity must be relativistic and sufficiently high ($a_0 \gg 1$) to expel most of the electrons out of the focal spot (Glinec *et al.*, 2005; Geissler *et al.*, 2006; Pukhov *et al.*, 2006; Banerjee *et al.*, 2012; Thomas *et al.*, 2014). Elliptical shape was introduced for the bubble by Sadeghi (Lu *et al.*, 2007; Bonabi *et al.*, 2009).

An important property of this regime is the production of mono-energetic high-quality electron beams. These electron beams are produced in the tail of the bubble trailing the relativistic intense laser pulse. Electrons can be trapped at the back of the cavity and accelerated by the longitudinal high-electric field (the space-charge force) until they reach the middle of the cavity where they start to decelerate. In addition to the longitudinal force responsible for the acceleration discussed above, the spherical (elliptical) shape of the ion cavity produces the transverse storing electric field. Therefore, electrons trapped and accelerated in the cavity are also transversally wiggled, so a collimated beam of X-ray radiation is emitted by this electron bunch. This radiation, which can be directly compared with a synchrotron emission in the wiggler regime, is called betatron radiation (Kiselev *et al.*, 2004; Rousse *et al.*, 2004).

Bubble shape and dimensions are important parameters for trapping and accelerating the background plasma electrons. Nonlinear evolution of the driver causes variations in the bubble shape, which triggers injection of ambient plasma electrons, resulting in the formation of a collimated, high-energy, quasi-mono-energetic electron beam (Xie *et al.*, 2007). Slow evolution of the self-guided pulse causes variations of the bubble shape and wake potentials. Therefore, understanding the self-injection or external injection process and its relation to nonlinear relativistic optical dynamics of the driver is vital for the production of high-quality beams. As an initially focused laser diffract, the bubble expands and electrons are injected continuously. It was shown analytically and by particle-in-cell (PIC) simulations that self-injection of the background plasma electrons into the quasi-static plasma bubble can be caused by the slow temporal expansion of the bubble (Kalmykov *et al.*, 2009, 2011).

In this paper, a new analytical formalism is introduced which is aimed at balancing the pondermotive force of the laser pulse and the electrostatic force of the bubble on its front boundary. In this formalism ellipsoid bubble dimensions are related to the laser pulse and plasma parameters.

Address correspondence and reprint requests to: Saeed Mirzanejhad, Department of Atomic and Molecular Physics, Faculty of Basic Science, University of Mazandaran, Babolsar, Iran. E-mail: saeed@umz.ac.ir

In Section 2, analytical formalism for bubble formation behind the laser pulse is established. The twofold ellipsoid structure of the bubble (egg shape) with compressed front and stretched rear side is established in this section. In Section 3, the relationship between the longitudinal and transverse bubble radiuses, R_z and R_r are found as a function of normalized maximum laser pulse amplitude a_0, pulse length l_p, laser beam waist w_0, and its normalized frequency ω/ω_p (plasma density scale). Further on, a numerical fitting procedure is introduced to define the functional dependency of the ellipsoid bubble's dimensions to the plasma and laser pulse parameters. In Section 6, concluding remarks are presented.

2. ELLIPSOID BUBBLE FORMATION

In this section, bubble formation next to the intense laser pulse is analyzed by a simple analytical description. In the bubble regime, a cavity free from electrons is formed behind the laser pulse instead of the plasma wave. In this regime, the electron dynamics are defined by the pondermotive force of the laser pulse and electromagnetic fields of the bubble. Correctly, the bubble includes the cavity with the large ion charge, the electrons sheath around the cavity forming the bubble boundaries, and the bunch of accelerated electrons at the base of the cavity. At the beginning of the interaction, there is no bunch yet, and the cavity shape is determined only by the pondermotive potential of the laser pulse. The transverse size of the cavity reaches a maximum near the middle plane which passes through the cavity center. The bubble moves through the plasma background with the group velocity of the laser pulse. In the excess of the laser pulse and bubble fields, the plasma background's ions are stationary due to its large mass approximately. But the plasma electrons are expelled by the pondermotive force. On the bubble boundary, the pondermotive force on the electrons in the definite distance from the laser axis is nearly balanced by the attracting force of the bubble. These electrons remain on the sheath around the bubble and make the bubble boundaries. In continue, we will focus on these electrons and write an expression for balancing the forces on them.

Electric and magnetic fields of the ellipsoid bubble which move with group velocity of the laser pulse are (Zobdeh *et al.*, 2009; Bonabi *et al.*, 2009),

$$E_x = \frac{{\beta_0}^2 x}{2(1+\beta_0)}, E_y = \frac{{\beta_0}^2 y}{2(1+\beta_0)}, E_z = \frac{\beta_0 \xi}{1+\beta_0}. \\ B_x = E_y, B_y = -E_x, B_z = 0. \tag{1}$$

In which variables are normalized as follows:

$$\tilde{E}\,(,\tilde{B}) = \frac{eE\,(,B)}{m_0 c \omega_p}, \quad \tilde{x} = k_p x, \tilde{y} = k_p y, \\ \tilde{\xi} = k_p \xi, \quad \tilde{t} = \omega_p t, \quad \tilde{\upsilon}_0 = \beta_0 = \frac{\upsilon_0}{c}, \tag{2}$$

and $\xi = z - \upsilon_0 t$, is the bubble-moving coordinate and $v_0 = c\,(1–\omega_p^2/\omega^2)^{1/2}$ is the group velocity of the laser pulse. We assume that the bubble center is located at origin in $t = 0$ (its center remains at $\xi = 0$ for all time). For this situation, the normalized longitudinal and transverse electromagnetic force components of the bubble on the test electron are,

$$F_{bub}{}^r = -\frac{{\beta_0}^2 r}{2(1+\beta_0)}, F_{bub}{}^z = -\frac{\beta_0 \xi}{1+\beta_0}. \tag{3}$$

Furthermore, we assume the normalized vector potential of the laser pulse with longitudinal and transverse Gaussian profiles as,

$$A_0(x,y,z,t) = a_0 \frac{w_0}{w(z)} exp\left[-\frac{r^2}{w^2(z)}\right] \\ \times exp\left[-\frac{4(\zeta-\zeta_0)^2}{l p^2}\right], \tag{4}$$

where

$$w(z) = w_0\sqrt{1+\frac{4(z-z_{0g})^2}{k^2 {w_0}^4}}, \quad r^2 = x^2+y^2, \\ \zeta_0 = z_{0l}, \quad z_{0l} = z_{0g} = z_0. \tag{5}$$

We assume, for simplicity, that the center of the laser pulse z_{0l} is located at the Gaussian beam waist z_{0g}, at $t = 0$. The pondermotive force can be expressed by $\vec{F}_{pond} = -\nabla V_{pond}$ (x, y, z, t), in which the normalized pondermotive potential is defined as,

$$V_{pond} = \left[\sqrt{1+\frac{\left|\vec{A}\,(x,y,z,t)\right|^2}{2}} - 1\right]. \tag{6}$$

In this manner, the normalized longitudinal and transverse components of the scattering pondermotive force are obtained as follows:

$$F_{pond}{}^r = -\frac{\partial}{\partial r} V_{pond} = -\frac{|A|}{2\sqrt{1+|A|^2/2}} \frac{\partial |A|}{\partial r} \\ = \frac{|A|^2 r}{w^2(z)\beta_0\sqrt{1+|A|^2/2}},$$

$$F_{pond}{}^z = -\frac{\partial}{\partial z} V_{pond} = -\frac{|A|}{2\sqrt{1+|A|^2/2}} \frac{\partial |A|}{\partial z} \\ = \frac{2|A|^2}{\beta_0\sqrt{1+|A|^2/2}}\left[\frac{(z-z_0 g)}{k^2 {w_0}^2 w^2(z)}\left(1-\frac{2r^2}{w^2(z)}\right) + \frac{2(\zeta-\zeta_0)}{l p^2}\right]. \tag{7}$$

Moreover, in the bubble regime of the LWFA, the bubble structure passing through the background plasma with the

https://doi.org/10.1017/S026303461600001X Published online by Cambridge University Press

group velocity of the laser pulse. In the equilibrium (quasi-static) state, some background electrons lay in the electron sheath layer around the bubble boundaries. These electrons introduce an electron sheath around the bubble which shield electrostatic field of the bubble out of the bubble boundaries. Of course, some of these electrons trap and accelerate toward the longitudinal axis in the rear part of the first bubble. In the laboratory reference frame, the electrons in the inner boundary of this sheath are in quasi-equilibrium in the longitudinal direction when they go along the sheath layer of the bubble. Now parameter α defines as follows to indicate longitudinal force balance condition for the electrons on the bubble boundaries,

$$\alpha = F_{\text{bub}}{}^{z} + F_{\text{pond}}{}^{z}. \tag{8}$$

Adiabatic variation of the bubble shape through the interaction of intense laser pulse is neglected in our equilibrium condition, and the bubble is assumed in a steady-state situation.

In the next section, we will follow numerical results for the derivation of spatial points around the driver laser pulse which have minimum values of parameter α. In this new formalism, the ellipsoid boundary in the front side of the bubble (interaction zone with laser pulse) is recognized. The rear side of the bubble has an ellipsoid structure with an approximately identical transverse radius but with different (stretched) longitudinal radius, R'_z. Figure 1 shows this structure by a cylindrical 2D simulation (Fig. 1 from Benedetti *et al.*, 2013). We obtain longitudinal and transverse radiuses of the bubble front side (R_z, R_r), and compare them with simulation results of this recent work. This twofold ellipsoid structure was observed in other multidimensional simulation results (see, for example, Pukhov & Meyer-Ter-vehn, 2002; Kostyukova *et al.*, 2004; Kalmykov *et al.*, 2011; Cowan *et al.*, 2012; Benedetti *et al.*, 2013). Asymmetric behavior of the ellipsoid in the front and rear sides is a consequence of the misallocation of the laser center with the ellipsoid's center. Discontinuity and scattering of the electrons in this point was shown in previous multidimensional simulations (Wu *et al.*, 2009; Cowan *et al.*, 2012; Kalmykov *et al.*, 2012).

In the next section, we obtain the analytical form of the R_z and R_r, as a function of the normalized laser pulse amplitude a_0, pulse length l_p, laser beam waist w_0, and its normalized frequency ω/ω_p (plasma density scale).

3. NUMERICAL RESULTS

In this section, ellipsoid dimensions are obtained as a function of laser amplitude a_0, waist w_0, pulse length l_p, and normalized frequency ω/ω_p (which defines plasma density). For each value of these parameters, the location of points in the front side of the bubble boundaries is obtained by numerical minimization of α Eq. (8). After each minimization procedure, ellipsoid equation $y^2/R_r^2 + z^2/R_z^2 = 1$ is fitted on these points. In this equation, R_r and R_z are transverse

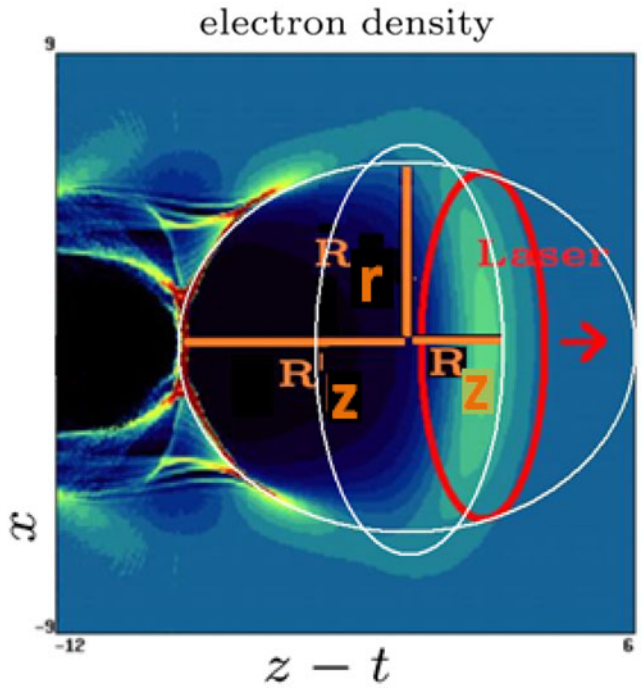

Fig. 1. The twofold (egg shape) ellipsoid structure of the bubble in highly nonlinear regime of LWFA by 2D simulation from Benedetti *et al.*, 2013. R_r is the transverse radius and R_z (R'_z) is the longitudinal radius of the front (rear) side of the bubble. Allocation of laser pulse and its orientation approximately are illustrated by the red curve and two ellipsoids are drawn with white curves.

(radial) and longitudinal radiuses of the ellipsoid bubble, respectively. For simplicity, in numerical results we assume that $t = 0$, center of the laser pulse and its beam waist are located at, $z_{0l} = z_{0g} = z_0$.

In the first step, we assume that ellipsoid cavity has enough large dimensions which spread all considered space, but in continue ellipsoid dimensions are obtained. Longitudinal force α is plotted in Figure 2 for some values of z_0, distance between laser pulse and bubble centers.

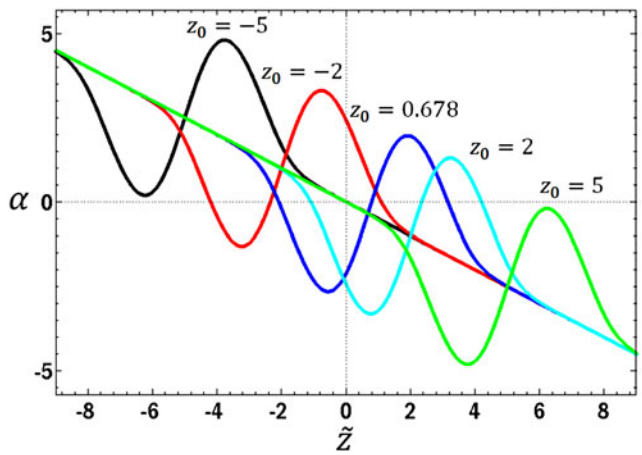

Fig. 2. Total longitudinal force α, for different z_0. Maximum slope occurred for $z_0 = 0.678$ at equilibrium condition, $\alpha = 0$.

https://doi.org/10.1017/S026303461600001X Published online by Cambridge University Press

In this figure, center of ellipsoid cavity is located at the origin and laser pulse is located at the front (rear) of bubble, $z_0 > 0$ ($z_0 < 0$). For each value of z_0, the longitudinal force has maximal three roots. First root (z_1 at the front of the cavity) shows the stable equilibrium point for allocation of electron sheath in front boundary of the ellipsoid cavity. Background plasma electrons in this point experience restoring force which returns any longitudinal displacement from equilibrium.

In continue, we obtain feasible value for z_0, in which maximum restoring force or maximum stability is occurred. Figure 3 shows the slope of the longitudinal force$d\alpha/dz|z_1$, at the first root, as a function of z_0. Equilibrium with the maximum stability occurred for $z_0^{\max}$, in which $|d\alpha/dz|$ is maximized. In this formalism, distance between the ellipsoid and laser pulse centers z_0, and longitudinal radius of the ellipsoid $R_z = z_1$ are obtained simultaneously. Transverse radius of the ellipsoid is obtained by a fitting procedure of the spatial points in the r–z plane for which α is minimized. In the fitting procedure, R_z (and z_0) is known by the above-mentioned method and suitable value of R_r is obtained by fitting ellipsoid equation. With this formalism, ellipsoid dimensions and its location are obtained in the wide range of the interaction parameters.

Figure 4a shows spatial points in the r–z plane for which α is minimized for normalized laser parameters $l_p = 2.0$, $w_0 = 3.6$, $\omega/\omega_p = 10$, and for different values of the normalized laser amplitude between 2 and 20. For small values of laser amplitude ($a_0 < 2$), there is no suitable numerical solution. This result is in good agreement with nonlinear the relativistic nature of the wake-field acceleration in the bubble regime ($a_0 > 1$).

In figure 4b, ellipsoid parameters are shown as a function of normalized laser amplitude a_0. Bubble dimensions interpolates by the following polynomials:

$$R_z(a_0) = \begin{cases} 0.6508\ a_0 - 0.1536, & 2 < a_0 \le 10, \\ 0.033\ a_0 + 5.896, & a_0 > 10\ . \end{cases}$$

$$R_r(a_0) = -0.021\ a_0^2 + 0.8622\ a_0 + 1.942.$$

$$z_0(a_0) = \begin{cases} 0.6183\ a_0 - 1.099, & 2 < a_0 \le 10, \\ 5 & a_0 > 10 \end{cases}. \qquad (9)$$

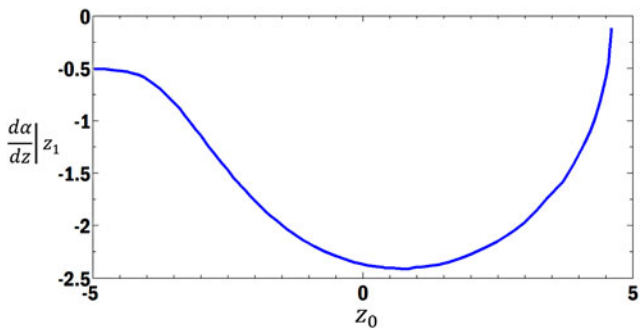

Fig. 3. Slope of the restoring force at the equilibrium for different z_0 values.

It is clear that the bubble has minimum dimensions in the moderate relativistic case, $R_r = 3.58$ and $R_z = 0.977$ (at $a_0 \gtrsim 2$), and then it grows asymptotically, with increasing laser amplitude throughout the highly relativistic regime, $R_r = 10.8$ and $R_z = 6.5$ ($a \approx 20$). For all laser amplitudes, the radial diameter is greater than the longitudinal diameter (oblate bubble), and the laser pulse locates in the front of the bubble center, $Z_0(a_0) > 0$.

In this step, we compare variation of the ellipsoid radius in terms of the laser pulse amplitude with the 2D PIC simulation results in Benedetti *et al.*, 2013. Linear fitting of our results in the defined range of the laser amplitude ($2 < a_0 < 7$) in this reference are presented in Figure 5. Linear fitting of the transverse radius is in agreement with the linear fitting of the PIC simulation in the prescribed range (Fig. 5a), but a big difference exists for the longitudinal radius (Fig. 5b). This difference between the rear and front ellipsoid longitudinal radiuses distinguished in the cavity structure obtained in 2D results of the PIC simulation in Figure 1. Comparison between these results (fig. 5b) shows that the rear side radius is approximately, few times greater than the front side of the bubble.

Figure 6a shows the bubble parameters (vs.) the different normalized laser pulse length ($1 < k_p l_p < 6$) for $a_0 = 10$, $w_0 = 3.6$, *and* $\omega/\omega_p = 10$. It is known that the resonance condition in the bubble regime is occurred for $l_p \approx \lambda_p/2$. Our numerical minimization procedure has failed for the laser pulses shorter than $\lambda_p/6$ ($k_p l_p < 1$)($k_p l_p < 1$.

Multiple definition functions are fitted for the bubble dimensions. Breaking at $k_p l_p \approx 2$ ($l_p \approx \lambda_p/3$), indicates the resonance condition for the pulse length, where bubble reaches to its maximum dimensions.

$$R_z(l_p) = \begin{cases} 0.465\ l_p + 5.273, & l_p \le 2, \\ 12.28\ l_p^{-0.8523} - 0.5665, & l_p > 2, \end{cases}$$

$$R_r(l_p) = \begin{cases} 12, & l_p \le 1.5, \\ 21.85\ l_p^{-1.743} + 1.419, & l_p > 1.5. \end{cases} \qquad (10)$$

Figure 7 shows the bubble parameters (vs.) the different laser spot size (w_0) for $l_p = 2.0$, $a_0 = 10$, *and* $\omega/\omega_p = 10$. It must be mentioned that the numerical procedure does not have a suitable solution beyond the prescribed range ($3.0 < w_0 < 4.2$) which is in agreement with optimum condition on the laser beam waist, $k_p w_0 = \sqrt{a_0} = 3.16$, for bubble excitation. Noticably, bubble structure exchanges from oblate to prolate for $w_0 \le 3$.

subsequently, linear functions are fitted on the bubble dimensions in figure 5,

$$R_z(w_0) = 6.2,$$

$$R_r(w_0) = -0.9041\ {w_0}^2 + 10.08\ w_0 - 16. \qquad (11)$$

Finally, Figure 8 shows the bubble dimensions (vs.) the different normalized laser frequency (ω/ω_p) for $l_p = 5.1$,

https://doi.org/10.1017/S026303461600001X Published online by Cambridge University Press

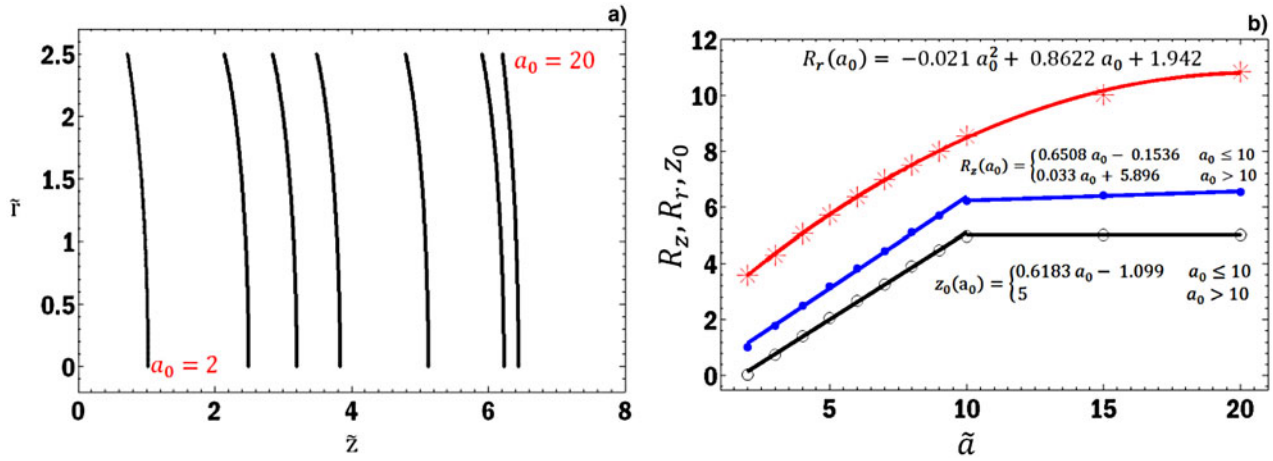

Fig. 4. (a) Bubble boundary in the r–z plane for different values of the normalized laser pulse amplitude. (b) Bubble dimensions as a function of the laser amplitude ($l_p = 2.0$, $w_0 = 3.6$, $\omega/\omega_p = 10$).

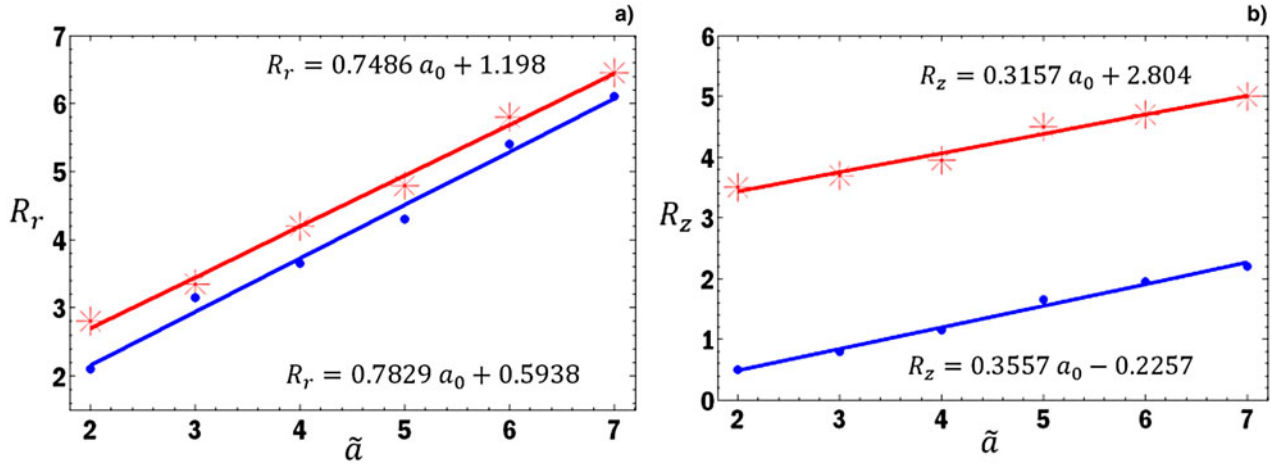

Fig. 5. Transverse (a) and longitudinal (b) radiuses of the bubble in terms of the normalized laser pulse amplitude from our formalism (blue line) and 2D PIC results (red dashed line) from Benedetti *et al.* (2013).

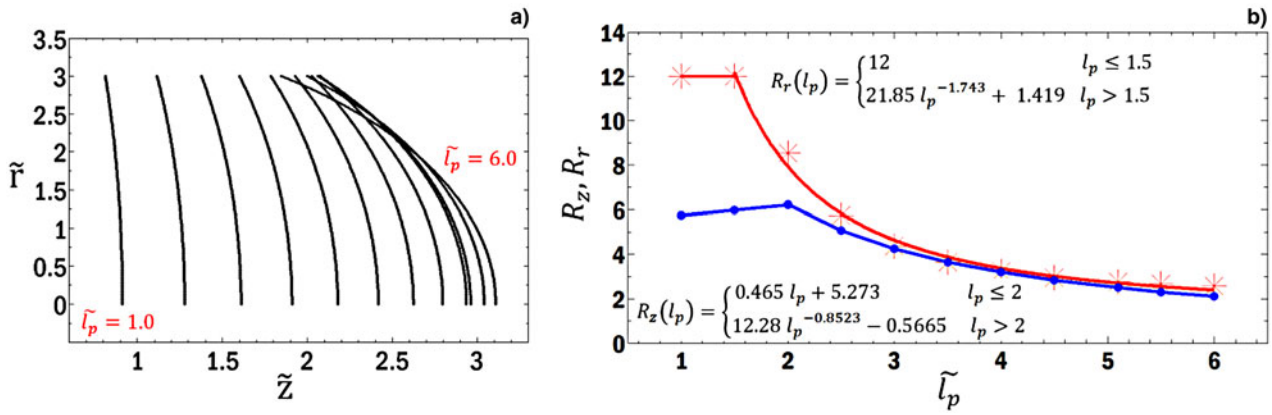

Fig. 6. (a) Bubble boundary in the r–z plane for different values of laser pulse duration. (b) Bubble dimensions as a function of pulse duration ($a_0 = 10$, $w_0 = 3.6$, $\omega/\omega_p = 10$).

https://doi.org/10.1017/S026303461600001X Published online by Cambridge University Press

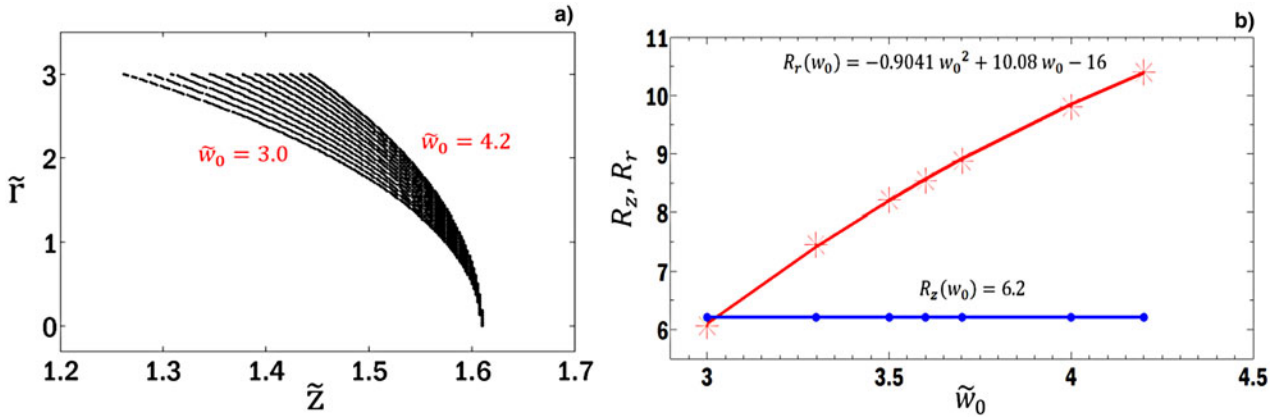

Fig. 7. (a) Bubble boundary in the r–z plane. Numerical allowed spot size range (3.0–4.2) is in good agreement with optimum bubble creation condition, $k_p w_0 = \sqrt{a_0} = 3.16$. (b) Bubble dimensions as a function of beam waist ($l_p = 2.0$, $a_0 = 10$, $\omega/\omega_p = 10$).

$a_0 = 10$, *and* $w_0 = 3.6$. Normalized laser frequency identifies plasma density scale (relative to the critical density). Subsequently, power dependencies are fitted suitably on the points,

$$R_r\left(\frac{\omega}{\omega_p}\right) = 3.547\left(\frac{\omega}{\omega_p}\right)^{-2.319} + 8.542,$$

$$R_z\left(\frac{\omega}{\omega_p}\right) = 0.688\left(\frac{\omega}{\omega_p}\right)^{-3.19} + 6.207. \qquad (12)$$

Ellipsoid bubble dimensions reach the values $R_r \simeq 8.5$ and $R_z \simeq 6.2$, asymptotically for dilute plasma ($\omega/\omega_p \gg 1$). However, its dimensions increase with decreasing laser frequency (or increasing plasma density) up to a near-critical condition ($\omega/\omega_p > 1$), to $R_r \simeq 12.1$ and $R_z \simeq 6.9$. Furthermore, the front side of the bubble remains oblate for all selected parameters.

By combining Eqs. (9)–(12), the bubble parameters have the following dependency to the laser characteristics, for two cases:

$$R_z\begin{cases} l_p \le 2, \begin{cases} a_0 \le 10 \\ a_0 > 10 \end{cases} \\ l_p > 2, \begin{cases} a_0 \le 10 \\ a_0 > 10 \end{cases} \end{cases} \text{and } R_r\begin{cases} l_p \le 1.5 \\ l_p > 1.5 \end{cases}.$$

$$R_z\left(a_0, l_p, \frac{\omega}{\omega_p}\right) = -1.1834 + 0.6508 a_0 + 0.465 l_p + 0.688\left(\frac{\omega}{\omega_p}\right)^{-3.19} \quad (\text{for } a_0 \le 10, l_p \le 2),$$

$$R_z\left(a_0, l_p, \frac{\omega}{\omega_p}\right) = 4.9516 + 0.033 a_0 + 0.465 l_p + 0.688\left(\frac{\omega}{\omega_p}\right)^{-3.19} \quad (\text{for } a_0 > 10, l_p \le 2),$$

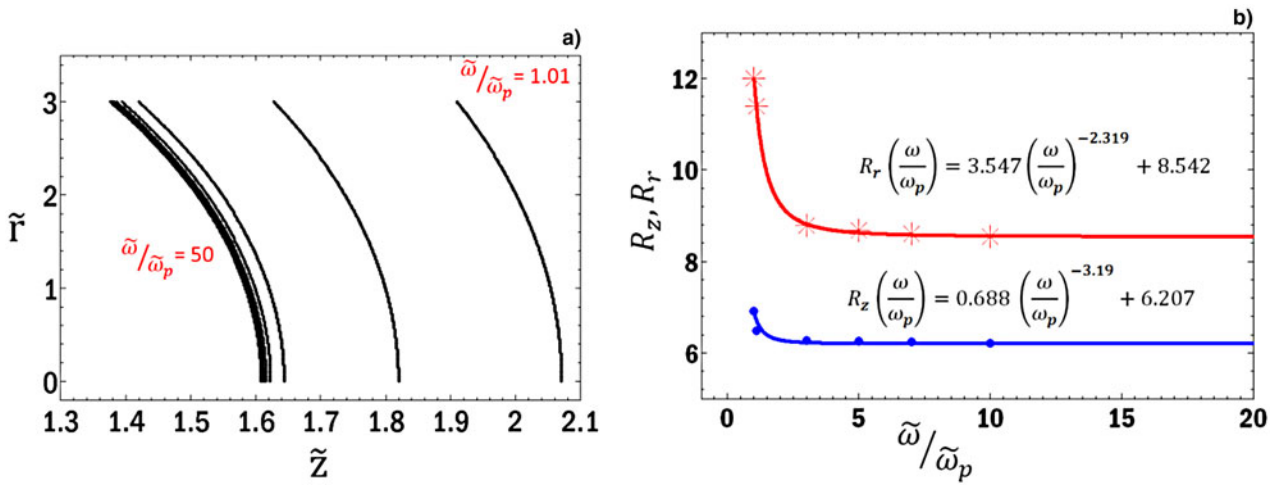

Fig. 8. (a) Bubble boundary in the r–z plan. (b) Bubble dimensions as a function of normalized laser frequency ($l_p = 2$, $a_0 = 10$, $w_0 = 3.6$). Bubble dimensions are minimized ($R_r \simeq 8.5$ and $R_z \simeq 6.2$) for the dilute plasma ($\omega/\omega_p > 10$).

https://doi.org/10.1017/S026303461600001X Published online by Cambridge University Press

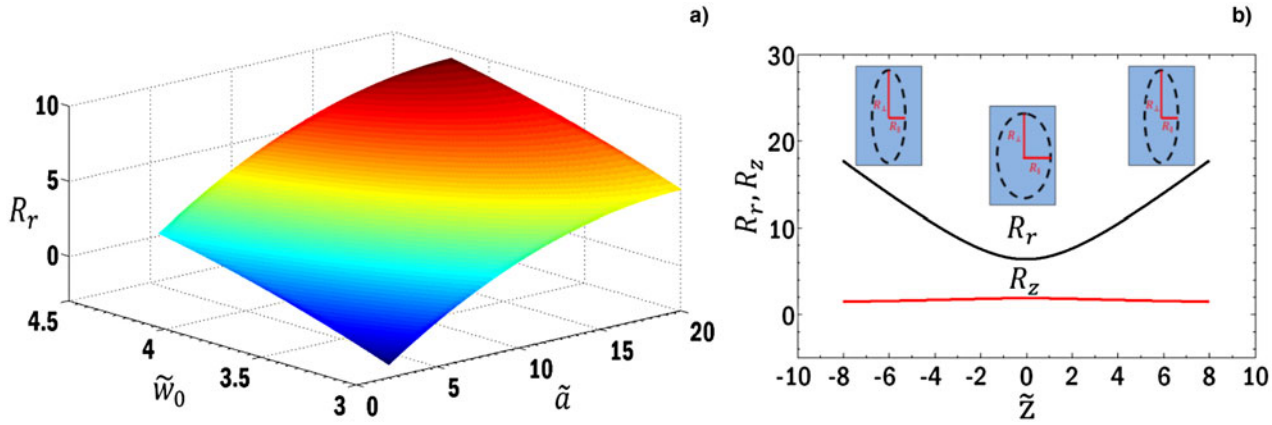

Fig. 9. (a) Transverse radius of the bubble in terms of normalized laser pulse amplitude and beam waist. (b) The schematic deformation of the bubble trough the propagation of a Gaussian laser pulse.

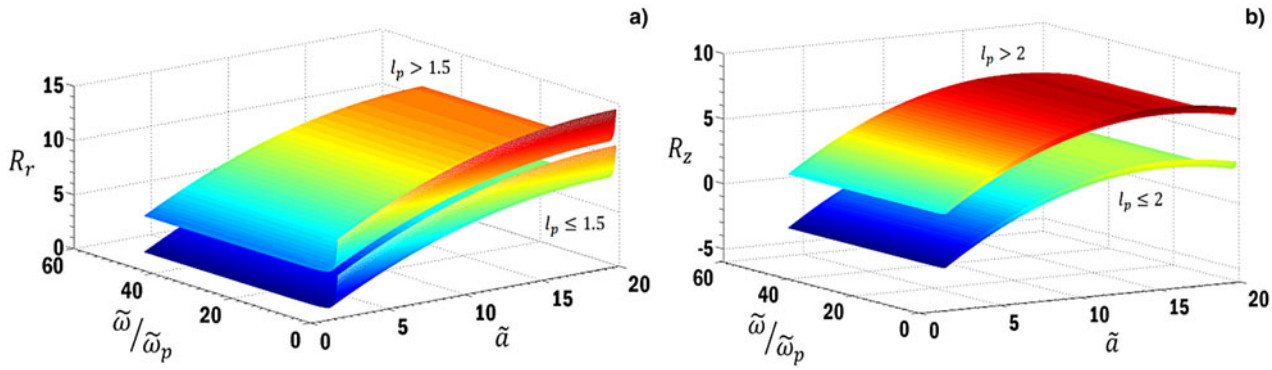

Fig. 10. Transverse (a) and longitudinal (b) radiuses of the bubble in terms of normalized laser pulse amplitude and frequency.

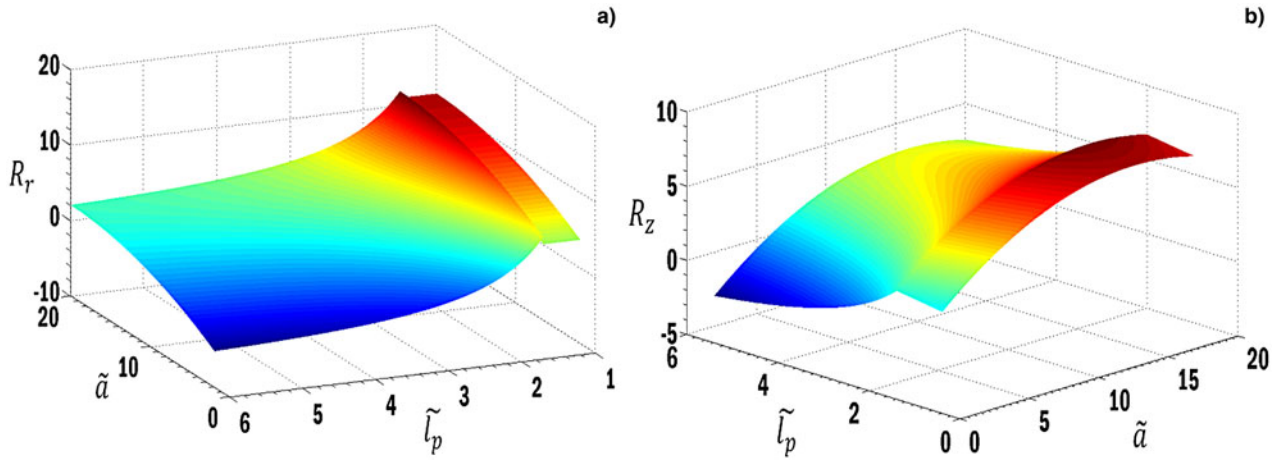

Fig. 11. Transverse (a) and longitudinal (b) radiuses of the bubble in terms of the normalized laser pulse amplitude and the laser pulse duration.

https://doi.org/10.1017/S026303461600001X Published online by Cambridge University Press

$$R_z\left(a_0, l_\mathrm{p}, \frac{\omega}{\omega_\mathrm{p}}\right) = -7.0445 + 0.6508a_0 + 0.688\left(\frac{\omega}{\omega_\mathrm{p}}\right)^{-3.19} + 12.28l_\mathrm{p}^{-0.8523} \quad (\text{for } a_0 \le 10,\ l_\mathrm{p} > 2),$$

$$R_z\left(a_0, l_\mathrm{p}, \frac{\omega}{\omega_\mathrm{p}}\right) = -0.9093 + 0.033a_0 + 0.688\left(\frac{\omega}{\omega_\mathrm{p}}\right)^{-3.19} + 12.28l_\mathrm{p}^{-0.8523} \quad (\text{for } a_0 > 10,\ l_\mathrm{p} > 2),$$

$$R_r\left(a_0, w_0, \frac{\omega}{\omega_\mathrm{p}}\right) = -22.58 - 0.021a_0^2 + 0.8622a_0 - 0.9041w_0^2 + 10.08w_0 + 3.547\left(\frac{\omega}{\omega_\mathrm{p}}\right)^{-2.319} \quad (\text{for } l_\mathrm{p} \le 1.5),$$

$$R_r\left(a_0, l_\mathrm{p}, w_0, \frac{\omega}{\omega_\mathrm{p}}\right) = -32.44 - 0.021a_0^2 + 0.8622a_0 - 0.9041w_0^2 + 10.08w_0 + 3.547\left(\frac{\omega}{\omega_\mathrm{p}}\right)^{-2.319} + 21.85l_\mathrm{p}^{-1.743} \quad (\text{for } l_\mathrm{p} > 1.5). \tag{13}$$

Figure 9a shows the variation of transverse radius of the bubble in terms of normalized laser pulse amplitude and beam waist. In figure (9b), the schematic deformation of the bubble is shown through the propagation of a Gaussian laser pulse in many Rayleigh lengths around the focus point. The ellipsoid bubble remains oblate in this path, but its compression is minimized in focus.

Figure 10 shows ellipsoid bubble radiuses as a function of normalized laser pulse amplitude and frequency. A great variation of the bubble dimensions in the moderate relativistic amplitude and near-critical plasmas ($\omega/\omega_\mathrm{p} \gtrsim 1$) reaches to the stable dimensions in the highly relativistic amplitude and dilute plasmas asymptotically ($\omega/\omega_\mathrm{p} \gg 1$).

Figure 11 shows bubble dimensions as a function of the normalized laser pulse amplitude and pulse length. Disconnection in the curves is occurred around the resonance condition, $k_\mathrm{p}l_\mathrm{p} \approx 2$ ($l_\mathrm{p} \approx \lambda_\mathrm{p}/3$).

4. CONCLUSION

In this paper, the variation of the ellipsoid bubble dimensions is investigated in a highly nonlinear regime of the LWFA (bubble regime). A new twofold ellipsoid structure of the bubble (egg shape) with a compressed front and a stretched rear side is suggested. This new twofold ellipsoid structure of the bubble is confirmed by referring to some published 2D and 3D simulations. Moreover, the slow evolution of the self-guided pulse causes variations of the bubble shape and wake potentials. It was shown analytically and by PIC simulations that self-injection of the background plasma electrons into the quasi-static plasma bubble can be caused by slow temporal expansion of the bubble (Kalmykov *et al.*, 2009, 2011).

In this paper, a new analytical formalism concerning the balancing of the pondermotive force of the laser pulse and the electrostatic force of the bubble is introduced. Accordingly, the relationship between the longitudinal and transverse bubble radiuses, R_z and R_r, is found as a function of the normalized laser pulse amplitude a_0, pulse length l_p, laser beam waist w_0, and its normalized frequency ω/ω_p (plasma density scale). It is shown that the longitudinal radius of the front side of the bubble is independent from the laser spot size w_0. Analytical functions $R_\mathrm{r}(a_0,\ w_0,\ l_\mathrm{p},\ \omega/\omega_\mathrm{p})$ and $R_z(a_0,\ l_\mathrm{p},\ \omega/\omega_\mathrm{p})$ are presented for the broad range of the laser and plasma parameters. This study revealed that, the front side of the ellipsoid bubble remains oblate for our selected parameters but exchanges to prolate at $k_\mathrm{p}w_0 \le 3$.

The ellipsoid bubble has minimum dimesnsions for small normalized laser pulse amplitude, $R_r = 3.58$ and $R_z = 0.977$ (moderate relativistic, $a_0 \gtrsim 2$), and then grows asymptotically with increasing laser amplitude throughout the highly relativistic regime ($a \gtrsim 20$), up to the normalized radiuses $R_r = 10.8$ and $R_z = 6.5$. Moreover, the linear fitting of our results is in good agreement with the linear fitting of the PIC simulation in Benedetti *et al.*, 2013, in the defined range of the laser amplitude ($2 < a_0 < 7$). Finally, ellipsoid bubble dimensions reach the values $R_r \simeq 8.5$ and $R_z \simeq 6.2$ asymptotically for dilute plasma ($\omega/\omega_\mathrm{p} \gg 1$), but its dimensions increase with decreasing laser frequency (or increasing plasma density up to a near-critical condition $\omega/\omega_\mathrm{p} \gtrsim 1$) to $R_\mathrm{r} \simeq 12.1$ and $R_z \simeq 6.9$.

The achieved analytical form of the ellipsoid bubble dimensions in the broad range of the laser and plasma parameters in this paper prepares a new ability for the analytical demonstration of the electron self-injection and acceleration in the bubble regime of the LWFA. Exact consideration of these processes is important for many research areas such as laser accelerators, high-quality x-ray sources, and high-energy particle colliders.

ACKNOWLEDGEMENT

The authors are grateful to Miss. Mahdieh Hamidzadeh for her collaborations.

REFERENCES

Banerjee, S., Powers, N.D., Ramanathan, V., Ghebregziabher, I., Brown, K.J., Maharjan, C.M., Chen, S., Beck, A., Lefebvre, E., Kalmykov, S.Y., Shadwick, B.A. & Umstadter, D.P. (2012). Generation of tunable, 100–800 MeV quasi-monoenergetic electron beams from a laser-wakefield accelerator in the blowout regime. *Phys. Plasmas* **19**, 056703.

Benedetti, C., Schroeder, C.B., Esarey, E., Rossi, F. & Leemans, W.P. (2013). Numerical investigation of electron self-injection in the nonlinear bubble regime. *Phys. Plasmas* **20**, 103108.

https://doi.org/10.1017/S026303461600001X Published online by Cambridge University Press

Bonabi, R.S., Navid, H.A. & Zobdeh, P. (2009). Observation of quasi-mono-energetic electron bunches in the new ellipsoid cavity model. *Laser Part. Beam* **27**, 223–231.

Cowan, B.M., Kalmykov, S.Y., Beck, A., Davoine, X., Bunkers, K., Lifshitz, A.F., Lefebvre, E., Bruhwiler, D.L., Shadwick, B.A. & Umstadter, D.P. (2012). Computationally efficient methods for modeling laser wakefield acceleration in the blow-out regime. *J. Plasma Phys*. **78**, 469–482.

Geissler, M., Schreiber, J. & Meyer-Ter-vehn, J. (2006). Bubble acceleration of electrons with few-cycle laser pulses. *New J. Phys*. **8**, 186.

Glinec, Y., Faure, J., Pukhov, A., Kiselev, S., Gordienko, S., Mercier, B. & Malka, V. (2005). Generation of quasi-monoenergetic beams using ultrashort and ultraintense laser pulses. *Laser Part. Beams* **23**, 161–166.

Kalmykov, S., Yi, S.A., Khudik, V. & Shvets, G. (2009). Electron self-injection and trapping into an evolving plasma bubble. *Phys. Rev. Lett*. **103**, 135004.

Kalmykov, S.Y., Beck, A., Davoine, X., Lefebvre, E. & Shadwick, B.A. (2012). Laser plasma acceleration with a negatively chirped pulse: All-optical control over dark current in the blowout regime. *New J. Phys*. **14**, 033025.

Kalmykov, S.Y., Beck, A., Yi, S.A., Khudik, V.N., Downer, M.C., Lefebvre, E., Shadwick, B.A. & Umstadter, D.P. (2011). Electron self-injection into an evolving plasma bubble: Quasi-monoenergetic laser-plasma acceleration in the blowout regime. *Phys. Plasmas* **18**, 056704.

Kiselev, S., Pukhov, A. & Kostyukov, I. (2004). X-ray generation in strongly nonlinear plasma waves. *Phys. Rev. Lett*. **93**, 135004.

Kostyukova, I., Pukhov, A. & Kiselev, S. (2004). Phenomenological theory of laser-plasma interaction in "bubble" regime. *Phys. Plasmas* **11**, 5256.

Lu, W., Tzoufras, M., Joshi, C., Tsung, F.S., Mori, W.B., Vieira, J., Fonseca, R.A. & Silva, L.O. (2007). Generating multi-GeV electron bunches using single stage laser wakefield acceleratio-nin a 3D nonlinear regime. *Phys. Rev. ST Accel. Beams* **10**, 061301.

Pukhov, A. & Gordienko, S. (2006). Bubble regime of wake field acceleration: Similarity theory and optimal scaling. *Phil. Trans. R. Soc. A* **364**, 623–633.

Pukhov, A. & Meyer-Ter-vehn, J. (2002). Laser wake field acceleration: The highly non-linear broken-wave regime. *Appl. Phys. B* **74**, 355–361.

Rousse, A., Phuoc, K.T., Shah, R., Pukhov, A., Lefebvre, E., Malka, V., Kiselev, S., Burgy, F., Rousseau, J.P., Umstadter, D. & Hulin, D. (2004). Production of a keV x-ray beam from synchrotron radiation in relativistic laser-plasma interaction. *Phys. Rev. Lett*. **93**, 135005.

Thomas, J., Pukhov, A. & Kostyukov, I.Y. (2014). Temporal and spatial expansion of a multi-dimensional model for electron acceleration in the bubble regime. *Laser Part. Beam* **32**, 277–284.

Wu, H.C., Xie, B.S., Liu, M.P., Hong, X.R., Zhang, S. & Yu, M.Y. (2009). Electron trajectories and betatron oscillation in the wake bubblein laser-plasma interaction. *Phys. Plasmas* **16**, 073108.

Xie, B.S., Wu, H.C., Wand, H., Wang, N.Y. & Yu, M.Y. (2007). Analysis of the electromagnetic fields and electron acceleration in the bubble regime of the laser-plasma interaction. *Phys. Plasmas* **14**, 073103.

Zobdeh, P., Bonabi, R.S. & Afarideh, H. (2009). Cavity generation and quasi-monoenergetic electron generation in laser–plasma interaction. *Phys. Part. Nucl. Lett*. **6**, 413–416.

https://doi.org/10.1017/S026303461600001X Published online by Cambridge University Press